IAOS

International Association for Obsidian Studies

Bulletin

Number 69   **Winter 2022**

CONTENTS

NEWS AND INFORMATION

IAOS Annual Meeting in Portland

Please join us for the IAOS meeting to be held during the Society for American Archaeology meeting in Portland, Oregon, USA. See your SAA conference program for location and meeting time.

CONSIDER PUBLISHING IN THE IAOS *BULLETIN*

The *Bulletin* is a twice-yearly publication that reaches a wide audience in the obsidian community. Please review your research notes and consider submitting an article, research update, news, or lab report for publication in the *IAOS Bulletin*. Articles and inquiries can be sent to IAOS.Editor@gmail.com Thank you for your help and support!

AN UPDATED VERSION OF ARCHAEOLOGICAL AGE COMPUTATION BASED ON OBSIDIAN HYDRATION

A new version of "Archaeological Age Computation Based on Obsidian Hydration: A Summary of the Current State of the Art," by Alexander K. Rogers and Christopher M. Stevenson, is **now available** for downloading. This document, first published in 2020 as a special issue of the *IAOS Bulletin*, has now been revised, updated, and retitled as "A Summary of Obsidian Hydration Dating Science and Method for Archaeologists" and incorporates advances of the last two years. Click **HERE** to download this latest edition.

NOTES FROM THE PRESIDENT

Hello IAOS members, and welcome to 2023. I hope everyone had a safe and happy holiday. There are several obsidian-related things to look forward to this year. First, please renew your IAOS membership dues. You can pay online on the IAOS main page. Membership dues allow the IAOS to host and assist conferences like the International Obsidian Conference (IOC), which will be held in Japan on July 3-6. The 2023 IOC organizers have created a Facebook page if you are interested in learning more about the conference. The link is https://www.facebook.com/profile.php?id=100088165880711.

This year, the IAOS is sponsoring a student to travel and present her research at the IOC. Rose Moir from McMaster University will be presenting on the characterization of obsidian artifacts from the Aegean. After attending, Rose will publish an excerpt of her presentation in the *IAOS Bulletin* and share her conference experience.

The Society for American Archaeology (SAA) meeting will be held in Portland, Oregon, on March 29 through April 2. The IAOS will have its yearly business meeting there. The time has not been announced, but once available, information will be on the IAOS website and in the SAA program. Also, the IAOS will award another Craig E. Skinner Best Poster Award at the Portland SAA conference.

In other news, Nico Tripcevich, Kyle Freund, and Lucas Johnson are finishing the 2021 IOC proceedings volume. It will be available from the University of California, Berkeley Archaeological Research Facility by late 2023. The volume includes obsidian research from Europe, Africa, Asia, Peru, Mexico, and the United States.

Also, in November 2022, Lucas Johnson and Marc Marino led an SAA webinar on the "Characterization of Obsidian and Coarse to Fine-Paste Ceramics with Handheld XRF."

Finally, please share your work with other obsidian researchers and students by submitting an article, research update, news, or lab report project to the *IAOS Bulletin*. You can send it directly to Carolyn Dillian via email at IAOS.Editor@gmail.com.

Sean Dolan, IAOS President
sgdolan@gmail.com

AN EQUATION RELATING OBSIDIAN HYDRATION RATE TO TEMPERATURE AND STRUCTURAL WATER CONTENT

Alexander K. Rogers[a] and Christopher M. Stevenson[b]

[a] Maturango Museum, Ridgecrest, California, USA
[b] Virginia Commonwealth University, Richmond, Virginia, USA

Abstract

Use of obsidian hydration for archaeological chronologies requires the determination of a hydration rate. This paper provides a detailed analysis of an equation relating intrinsic water content and temperature to hydration rate, where hydration is measured by optical microscopy. The equation is based on a least-squares best fit of a mathematical model to a set of published data (N = 29). The model for the temperature dependence is derived from kinetic theory of reactions, and the model for the dependence on water content is based on the mechanics of glass formation. The resulting equation is

$$k = \exp[36.29 - (10005 - 354*w)/T],$$

where k is hydration rate in $\mu^2/1000$ years, w is total structural water content in wt.%, and T is temperature in Kelvins. The equation gives valid hydration rates for archaeological temperatures, with $R^2 = 0.9998$ and accuracy ≈ 0.3427 $\mu^2/1000$ years, one-sigma (N = 6). The range of structural water values used in the fit is $0.1 < w < 1.02$ wt.% and the form of the equation conforms with expectations based on the physics of hydration. The wide range of temperatures in the data set (20°C to 180°C) provides a solid basis for verifying the form of the temperature variation. The concept of geochemical source and sub-source, as a proxy for controlling for structural water, has long been traditional in archaeological OHD analyses. However, geochemical sources have a range of water contents (and hence of hydration rates), which contributes to the uncertainty in computed age. This equation allows rate calculation for individual artifacts with measured water content, which improves age accuracy.

Introduction

Obsidian hydration dating (OHD) is based on computing the age of an obsidian artifact by measuring water absorption since the artifact was created, and is widely used archaeologically in the Great Basin and the Inter-Mountain West. Application of OHD requires, among other data, the determination of a hydration rate. The hydration rate, in turn, is known to be determined principally by two factors: an environmental factor, temperature; and a compositional factor, the intrinsic (or structural) water content. The standard OHD method today controls for water content by geochemical sourcing and assigning a common rate to all artifacts from that source; however, sourcing can only control for the mean water content of a source, while water content is also known to vary within a source (Stevenson et al. 1993). Such intra-source variation degrades the accuracy of the computed OHD age. Rogers and Stevenson (2022) analyzed the improvement in accuracy achievable by measuring the water content of each specimen and determining a rate on that basis, which requires an equation relating rate to water content. This paper describes in detail the derivation of that equation and quantifies the accuracy of the resulting hydration rate.

Geochemical studies have led to equations for the hydration (and out-gassing) rate of obsidian in terms of temperature, pressure, and intrinsic water content for temperatures and pressures of geological interest (Zhang et al. 1991; Zhang and Behrens 2000), but they do not extrapolate correctly to archaeological temperatures. This paper develops an alternative equation specifically for archaeological conditions. The data set is large (N = 29) and includes temperatures from 20°C to 190°C, replacing an earlier equation (Rogers 2015; Rogers and Stevenson 2017) which was based on a very small data set. The prior equation (referred to in this analysis as the "Current Fit") is

$$k=\exp(37.76–2.289*w–10433/T+1023*w/T) \quad (1)$$

where k is hydration rate in $\mu^2/1000$ years, w is total intrinsic (or structural) water in wt.%, and T is temperature in Kelvins. This equation followed the form proposed by Zhang et al. (1991), but with numerical constants adjusted for archaeological conditions. It has two drawbacks, however: first, the pre-exponential clearly depends on water content w, while Doremus (2002: 68ff) argued that the dependence should be only in the activation energy; second, the data set was small (N = 6) and the temperature variation was scaled from infrared (IR) transmission data. These concerns are resolved by the proposed equation herein.

For this analysis the hydration is assumed to be measured by depth of water penetration as determined by optical microscopy, since it is the standard in American archaeology today; experimental methods such as Secondary Ion Mass Spectrometry (SIMS) and measurement of water mass gain by IR spectrometry are not addressed. The analytic approach here postulates a functional form of the equation based on the physics of hydration in glass, and then develops a least-squares best fit to published data on water content and hydration rate. The model for the dependence of hydration rate on water content is based on the mechanics of glass formation, while the model for temperature dependence of hydration rate is derived from the kinetic theory of reaction rates. With the proposed equation the hydration rate can be estimated for any desired effective hydration temperature (EHT) at atmospheric pressure, if intrinsic water content is measured or known.

Water in Obsidian

All obsidians contain small amounts of natural water, known as intrinsic water or structural water, resulting from the magma formation process; the amount is generally < 2.5% by weight (wt.%) in natural obsidians, although cases of somewhat higher concentration are occasionally encountered (Newman et al. 1986: 1528, Table 1; Zhang et al. 1997: 3091). Obsidian forms from a melt which is primarily silica and alumina; the melt is a liquid, with no internal order at the molecular level. As the temperature decreases, the degree of order increases as the tetrahedral glass network starts to form. If there are no modifier ions present, the silica-alumina network forms with the interatomic spacing characteristic of its composition, about 0.086 nanometer (which Doremus [2002: 67], defined in terms of a "doorway radius"). Modifier ions present in the melt, such as water, cause the glass to form interstices around them (Shelby 2005: 145). The radius of a water molecule is in the range of 0.138 - 0.233 nanometer (Doremus 2002: 63), so the diameter is roughly 0.4 nanometer. This leads to much larger interstices than for the water-free case, with the larger interstices representing voids in the glass matrix and hence greater openness. Doremus (2002) argued that this should result in a decrease in activation energy (Doremus 2002: 138), and any such decrease in Q would lead to increased hydration rate (Garofalini 2020;

Kuroda et al 2018, 2019; Kuroda and Tachibana 2019).

Hydration Models

The temperature dependence of hydration rate can be described by the Arrhenius equation

$$k = \exp[A - Q/T] \tag{2}$$

where $k_0 = \exp(A)$ is the pre-exponential constant, Q is activation energy in Kelvins, and T is temperature in Kelvins (Doremus 2002; Friedman and Long 1976; Glickman 2000: 257). The discussion above of glass formation suggests that the activation energy Q is a function of water content, with increasing water content leading to lower activation energy. The form of such a dependence assumed here is the simple form suggested by Doremus (2002): a linear decrease with water content, or

$$Q = Q_0 - a*w$$

where a is a constant and w is total water in wt.%, leading to a 3-parameter linear fit in which rate is given by

$$k = \exp[A - (Q_0 - a*w)/T] \tag{3}$$

The three parameters A, Q_0, and a, are to be determined by the least-squares best fit process to a data set. Thus, given a data set for hydration rate (k) at a known temperature (T) and for a known water content (w), a least-squares best fit can be computed to determine the values of the constants.

Data Set

The data set as employed here is based on published data on two obsidian sources in eastern California: the Coso volcanic field in Inyo County and the Bodie Hills volcanic field in Mono County. The Coso volcanic field is known to include four geochemically distinct subsources (Hughes 1988) with differing hydration rates (Rogers 2011; Rogers and Yohe 2013; Stevenson et al. 2000). Bodie Hills, in turn, has been found to consist of two subsources with differing water contents and hydration rates (Stevenson et al. n.d.), although no geochemical distinction has been published.

The data set is made up of four distinct subsets: (1) laboratory hydration measurements for two Coso obsidian subsources (Stevenson and Scheetz 1989); (2) measurements of water content in all four Coso subsources (Stevenson et al. 1993;

Source	Temperature, °C	Hot-soak time, days	Hydration rim, μ
SLM	160	3	3.72
SLM	160	6	5.05
SLM	160	12	6.90
SLM	160	18	8.90
SLM	130	12	2.95
SLM	140	12	3.77
WSL	160	3	2.38
WSL	160	6	3.58
WSL	160	12	5.02
WSL	160	18	5.34
WSL	130	12	2.12
WSL	140	12	2.41

Table 1. Laboratory hydration data for Coso sources. WSL = West Sugarloaf, SLM = Sugarloaf Mountain (from Stevenson and Scheetz 1989; 25, Table 1)

Coso Source	Hydration rate, μ^2/1000 years at 20°C	Mean structural water content, wt.%
West Sugarloaf	18.16	0.62
Sugarloaf Mountain	29.87	1.02
Joshua Ridge	23.72	0.82
West Cactus Peak	29.58	1.01

Table 2. Coso archaeological hydration rates and water content. (Rogers 2008; Rogers and Yohe 2018; Stevenson et al. 1993)

Rogers 2008) combined with archaeologically-determined hydration rates for all four Coso subsources (Rogers 2015); (3) laboratory hydration data with aggregated measurements of water content for the two subsources in the Bodie Hills (Stevenson et al. n.d.); and (4) laboratory hydration data for two Bodie Hills specimens with specimen-specific water content data (Stevenson et al. n.d.).

For data subset (1), laboratory hydration measurements were made for specimens from Coso West Sugarloaf (WSL) and Coso Sugarloaf Mountain (SLM) by Stevenson and Scheetz (1989). Eight specimens from each source were subjected to a hot-soak in silica-buffered distilled water, quenched, and hydration rims measured. The temperatures ranged from 130°C to 190°C, and hot-soak times between three and eighteen days; the specimens subjected to 190°C could not be read due to diffuse hydration, so a total of fourteen valid data points resulted (Table 1). Water content was not measured for each specimen, but mean values can be inferred from published Coso data (Rogers 2008; Stevenson et al. 1993).

Archaeologically-determined hydration rates for the four Coso sources were published by Rogers and Yohe (2013) (data subset 2). They were determined by obsidian-radiocarbon association and comparison with laboratory data, and have proven to yield valid archaeological ages (Rogers and Yohe 2014; Rogers et al. 2018). Stevenson et al. (1993) measured structural water content for these same four Coso sources. Transmission IR spectrometry was used to measure IR absorbance of water species (OH and H_2O_m), and concentrations were computed by the Beer-Lambert law (Newman et al. 1986). The resulting data were re-analyzed by Rogers (2008) to determine statistics. Table 2 presents the combined data for water content and archaeological rate for the Coso sources. The data for West Cactus Peak are anomalous, in that the distribution of water content appears to be bimodal (Rogers 2008), so this source was not included in the best fit data set here. As a further caveat, it should be noted that the structural water data and hydration rates were not measured on the same specimen, so uncertainties due to intra-source water variation remain.

For the Bodie Hills volcanic field (data subset 3), measurements of structural water content by transmission IR spectrometry for a large data set (N = 114) showed that there are two sub-populations of differing water content (Stevenson et al. n.d.). Bodie Hills Group 1 (BH1) has a mean water content of 0.2078 ± 0.0616 wt.% (N = 27), while Bodie Hills Group 2 (BH2) has a mean water content of

Source	Water content, wt.%	Rate, μ^2/1000 yrs
BH1	0.2078	11.25
BH2	0.1125	10.00

Table 3. Group hydration rates for Bodie Hills obsidian at 20°C

Bodie Hills Group	Water content, wt.%	Hot-soak temperature, °C	Hot-soak time, days	Hydration rim, μ
BH1	0.1005	140	59.24654	6.64
BH1	0.1005	150	59.24654	8.86
BH1	0.1005	160	59.24654	10.42
BH1	0.1005	170	59.24654	14.40
BH1	0.1005	180	59.24654	16.23
BH2	0.2474	140	59.22571	5.91
BH2	0.2474	150	59.22571	7.75
BH2	0.2474	160	59.22571	9.96
BH2	0.2474	170	59.22571	13.29
BH2	0.2474	180	59.22571	18.09

Table 4. Hydration rate and water content data for Bodie Hills obsidian (from Stevenson et al. n.d.; Table 5)

0.1135±0.0354 wt.% (N = 87). The difference is statistically significant at the 95% confidence level, but there is no known geochemical signature to distinguish the two groups. These data provide two more data points (Table 3).

Finally, for data subset (4), hydration rates were measured by laboratory hydration on a specimen from each Bodie Hills group (Table 4).

For analysis purposes these data were assembled into a single set. Temperatures were converted from Celsius to Kelvin (K = C + 273.15), and hydration rates were computed from hydration rims and hot-soak times (k = r^2/t). Finally, the natural logarithm of rate was computed, for reasons discussed below. Table 5 shows the completed data set (N = 29).

An additional set of data was analyzed for possible inclusion (Mazer et al. 1991a, 1991b), which would have increased the sample size to 80. However, the hydration rate data (Mazer et al. 1991a; Table 2) are averages of multiple runs with differing water content, and a plot of rate vs. water content at 160°C showed the curve to exhibit significant scatter. When the data were incorporated into our Table 5 on a trial basis and the best fits computed, the root-mean-square (rms) residuals were more than doubled. Since the

original basic data of Mazer et al. (1991a, 1991b) were not published, there was no way to resolve the scatter, so these data were not included in the best fit analysis below.

Analytical Procedure and Results

The data set in Table 5 was used as an input to the curve-fitting routine in PSI-Plot (v. 9), by PolySoftware International. The software computes best-fit parameters for any specified equation and data set using the Levenberg-Marquardt algorithm, plus goodness-of-fit statistics. In running the best fit solutions, it was found that making the fit to ln(k) and then taking the exponential gave a more robust solution than fitting directly to k. The resulting best-fit valuers to the 3-parameter equation are: A = 36.289, Q_0 = 10005.011 K, and a = 353.932 K/wt.%. Rounding the Q_0 and a values, the best-fit equation is

$$ln(k) = 36.29 - (10005 - 353*w)/T \qquad (4)$$

where k is in $μ^2$/1000 years, T is in Kelvins, and w is total water in wt.%.

Goodness of fit is measured by two statistics, the rms residuals between the fit and the data, and Pearson's R^2. The initial fit was made with ln(k), so Table 6 shows the

Source	Water content, wt.%	T, ºC	T, K	t, days	Hydration rim,μ	Hydration rate, μ²/day	ln(rate)
SLM	1.02	160	433.15	3	3.72	4.6128	1.5288
SLM	1.02	160	433.15	6	5.05	4.2504	1.4470
SLM	1.02	160	433.15	12	6.90	3.9675	1.3781
SLM	1.02	160	433.15	18	8.90	4.4006	1.4817
SLM	1.02	130	403.15	12	2.95	0.7252	-0.3213
SLM	1.02	140	413.15	12	3.77	1.1844	0.1692
SLM	1.02	170	443.15	12	8.76	6.3948	1.8555
SLM	1.02	20	293.15	-	-	8.131E-05	-9.4172
WSL	0.62	160	433.15	3	2.38	1.8881	0.6356
WSL	0.62	160	433.15	6	3.58	2.1361	0.7590
WSL	0.62	160	433.15	12	5.02	2.1000	0.7420
WSL	0.62	160	433.15	18	5.34	1.5842	0.4601
WSL	0.62	130	403.15	12	2.12	0.3745	-0.9821
WSL	0.62	140	413.15	12	2.41	0.4840	-0.7257
WSL	0.62	170	443.15	12	4.82	1.9360	0.6606
WSL	0.62	20	293.15	-	-	4.966E-05	-9.9102
JR	0.81	20	293.15	-	-	6.494E-05	-9.6420
BH2	0.1005	140	413.15	59.22571	5.91	0.5897	-0.5281
BH2	0.1005	150	423.15	59.22571	7.75	1.0141	0.0140
BH2	0.1005	160	433.15	59.22571	9.96	1.6750	0.5158
BH2	0.1005	170	443.15	59.22571	13.29	2.9822	1.0927
BH2	0.1005	180	453.15	59.22571	18.09	5.5254	1.7094
BH2	0.1125	20	293.15	-	-	2.746E-05	-10.5028
BH1	0.2474	140	413.15	59.24654	6.64	0.7442	-0.2955
BH1	0.2474	150	423.15	59.24654	8.86	1.3250	0.2814
BH1	0.2474	160	433.15	59.24654	10.42	1.8326	0.6057
BH1	0.2474	170	443.15	59.24654	14.40	3.5000	1.2527
BH1	0.2474	180	453.15	59.24654	16.23	4.4460	1.4920
BH1	0.2078	20	293.15	-	-	3.075E-05	-10.3897

Table 5. Data set for best-fit analysis

goodness-of-fit measures for the fit to ln(k) for the full data set (N = 29). The 3-parameter fit clearly gives significantly improved performance in terms of both measures.

For archaeological purposes the goodness of fit with respect to the rate k is of more interest than with respect to ln(k). Here it is evaluated against the archaeologically-determined rates at 20°C from Tables 2 and 3; data for Napa Glass Mountain are from Rogers 2019, and the data for West Cactus Peak were excluded due to the anomalous water content data. Table 7 shows the hydration rates at 20°C computed by the four methods. Again, goodness-of-fit is measured by the root-mean-square residuals between the best fit and the

Statistic	Current Fit	3 Parameter Fit
R²	0.9929	0.9967
rms residuals	0.3442	0.2360

Table 6. Goodness-of-fit statistics for ln(k). (N = 29)

Source	Water content, wt.%	Archaeological rate	Current fit	3-parameter fit
Bodie Hills Group 2	0.113	10.00	10.032	9.930
Bodie Hills Group 1	0.208	11.25	11.248	11.141
Napa Glass Mountain	0.180	10.68	10.879	10.773
Coso West Sugarloaf	0.620	18.14	18.451	18.328
Coso Joshua Ridge	0.810	22.27	23.179	23.054
Coso Sugarloaf Mountain	1.020	29.87	29.827	29.709

Table 7. Archaeological rates compared with least-squares best fits (N = 6). (Rates in μ^2/1000 yrs. at 20°C)

archaeological rate, and by Pearson's R^2. (Table 8). Both fits have the same R^2 to four decimal places, but the 3-parameter fit has the better fit to this archaeological data set as indicated by the rms residuals.

In equation (4) the effects of structural water are confined to the activation energy term, as suggested by physics (Doremus 2002: 138). If w > 28 wt.%, equation (4) can yield a negative activation energy, which is physically impossible; however, obsidian with H_2O_t > 2.7 wt.% does not occur in nature (Zhang et. al. 1997: 3091), so this is not a practical concern archaeologically. Figure 1 shows its fit with the archaeological data.

Hydration Rate Accuracy

For any given value of T, the accuracy of rate computed by equation (4) is determined by the accuracy of the three constant parameters and the accuracy of measuring w. It is very likely that the parameter accuracies are correlated, so a simple "square root of the sum of the weighted squares" method is not appropriate. Instead, the effect of the accuracies of the parameters is assumed to be summarized by the rms residuals; the residuals can be combined with the accuracy in w, since water measurement is independent and not

correlated with the other parameters. By the propagation of error method (Taylor 1982), it can be shown from equation (4) that the contribution to the standard deviation of rate (σ_{kw}) due to errors in measuring water (σ_w) is

$$\sigma_{kw} = k*354*\sigma_w/T \qquad (5)$$

Then the overall accuracy of rate is

$$\sigma_k = sqrt[(\sigma_{kw})^2 + (\text{rms residuals})^2] \qquad (6)$$

Typical magnitudes of σ_w can be estimated from a data set (N = 114) for Bodie Hills, California (Stevenson et al. 2021; Stevenson et al. n.d.). The measurements were made by transmission IR spectroscopy at the 4500 cm^{-1} absorption band, and hence actually measure hydroxyl (OH) content; they are used here as a proxy for total water (w) content. The OH concentrations were computed by the Beer-Lambert law, while OH accuracies were computed by propagation of error methods and confirmed by a Monte Carlo simulation of errors (Table 9).

Examination of Table 9 shows that the σ_{OH} values fall in the range 0.0010 wt.% < σ_{OH} < 0.0035 wt.%, with a mean of σ_{OH} = 0.0016 wt.%. The contribution to rate error due to

Statistic	Current Fit	3 Parameter Fit
R^2	0.9998	0.9998
rms residuals	0.401	0.342

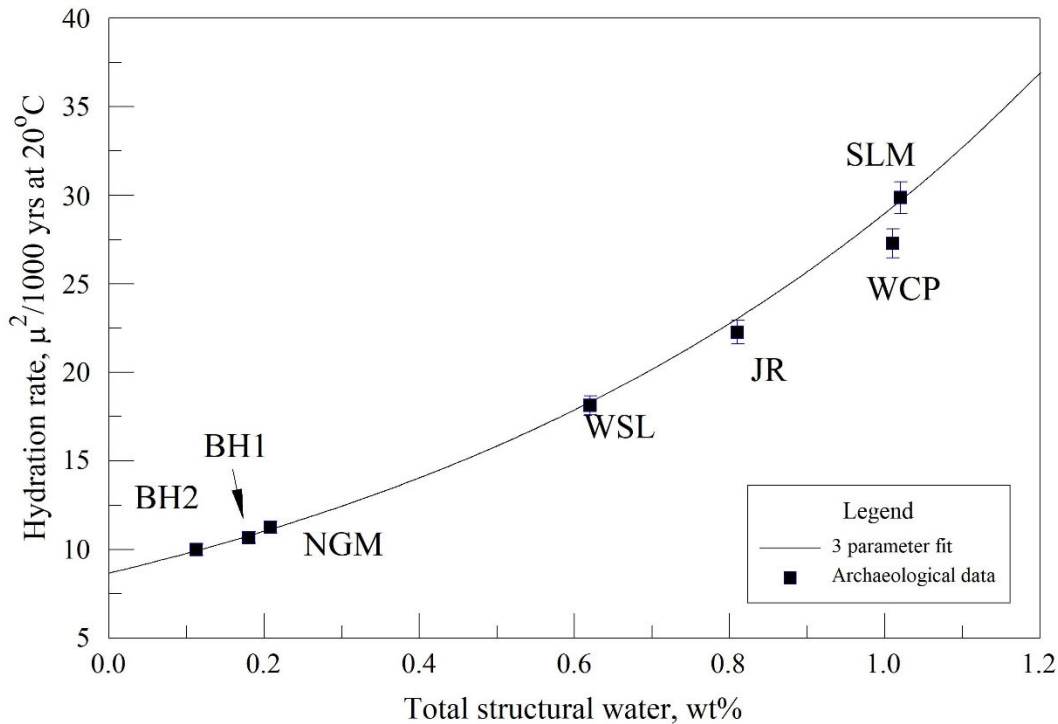**Table 8.** Goodness-of-fit to archaeological rates (N = 6)

Figure 1. Comparison of 3-parameter linear fit with archaeological data. Error bars on data points = 5%, typical of archaeological rates. Napa Glass Mountain and West Cactus Peak are shown for comparison but were not used in the best fit process. BH1 = Bodie Hills Group 1; BH2 = Bodie Hills Group 2; NGM = Napa Glass Mountain; WSL = Coso West Sugarloaf; JR = Coso Joshua Ridge; WCP = Coso West Cactus Peak; SLM = Coso Sugarloaf Mountain.

water content accuracy (σ_{kw}) at 20°C was computed by equation (5) for all the data points in Table 9, and lies between 0.0115 μ^2/1000 yrs. $< \sigma_{kw} <$ 0.0520 μ^2/1000 yrs. It is thus an order of magnitude smaller than the rms residuals (0.342 μ^2/1000 yrs.). After including the effects of σ_{kw} in equation (6), the σ_k values are found to be tightly clustered (0.3422 μ^2/1000 yrs. $< \sigma_k <$ 0.3459 μ^2/1000 yrs.), with a mean value of σ_k = 0.3427 μ^2/1000 years.

Discussion and Conclusion

The 3-parameter linear fit equation derived here (equation 4) is based on glass science and the known physical and chemical models of obsidian hydration. The data set is reasonably large (N = 29) and includes a wide range of temperatures (20°C to 180°C); the inclusion of archaeologically-derived rates is crucial to avoid extrapolation in extending the temperature range down to 20°C. This wide range of temperatures provides a solid basis for establishing the temperature variation of hydration rate, which is shown to follow the Arrhenius equation. Although the range of water content values is more limited (0.1 < w < 1.02 wt.%), the 3-parameter linear fit conforms with expectations based on the effects of structural water in hydration. Nevertheless, these results should be regarded as provisional until an extension of this analysis with a data set with a greater range of water content values is possible.

For practical archaeological application, the recommended equation relating water

Region	Specimen	A_{4500}	Density, gm/L	Thickness, cm	OH, wt.%	σ_{OH}, wt.%
BH-2	1A1	0.0439	2378	0.1459	0.1318	0.0016
BH-2	1B	0.0344	2379	0.1385	0.1088	0.0013
BH-2	1B	0.0344	2379	0.1385	0.1088	0.0013
BH-2	1C	0.0420	2379	0.1208	0.1523	0.0018
BH-2	1D	0.0252	2380	0.1063	0.1037	0.0013
BH-2	1E	0.0416	2379	0.1648	0.1105	0.0013
BH-2	1F	0.0380	2380	0.1507	0.1103	0.0013
BH-2	1G	0.0456	2381	0.1640	0.1216	0.0014
BH-2	1H	0.0388	2380	0.1438	0.1181	0.0014
BH-2	1I	0.0393	2380	0.1486	0.1158	0.0014
BH-2	1J	0.0438	2381	0.1612	0.1189	0.0014
BH-1	2D	0.0395	2380	0.1398	0.1236	0.0015
BH-1	2G	0.0557	2384	0.1067	0.2281	0.0027
BH-1	2H	0.0388	2381	0.1292	0.1314	0.0016
BH-1	2I	0.0501	2382	0.0976	0.2245	0.0026
BH-1	3B	0.0528	2381	0.1223	0.1889	0.0022
BH-1	3D	0.0494	2381	0.1209	0.1788	0.0021
BH-1	3H	0.0317	2379	0.1206	0.1151	0.0014
BH-1	3I	0.0873	2383	0.1285	0.2970	0.0035
BH-1	3J	0.0533	2384	0.1247	0.1868	0.0022
BH-1	4A	0.0504	2382	0.1192	0.1849	0.0022
BH-1	4C	0.0661	2381	0.1304	0.2217	0.0026
BH-1	4D	0.0641	2381	0.1253	0.2238	0.0026
BH-1	4E	0.0510	2380	0.1008	0.2214	0.0026
BH-1	4F	0.0589	2384	0.1142	0.2254	0.0026
BH-1	4G	0.0727	2384	0.1274	0.2494	0.0029
BH-1	4H	0.0612	2357	0.1231	0.2197	0.0025
BH-1	4I	0.0536	2383	0.1083	0.2163	0.0025
BH-1	5A	0.0544	2382	0.1510	0.1575	0.0018
BH-1	5B	0.0670	2380	0.1303	0.2250	0.0026
BH-1	5C	0.0487	2382	0.1476	0.1443	0.0017
BH-1	5D	0.0497	2382	0.1571	0.1384	0.0016
BH-1	5E	0.0495	2380	0.1403	0.1544	0.0018
BH-1	5F	0.0622	2380	0.1632	0.1668	0.0020
BH-1	5G	0.0689	2380	0.1520	0.1984	0.0023
BH-1	5H	0.0488	2380	0.1637	0.1305	0.0015
BH-1	5I	0.0432	2388	0.1130	0.1668	0.0020
BH-1	5J	0.0495	2385	0.1066	0.2028	0.0024
BH-2	6B	0.0322	2380	0.1075	0.1311	0.0016
BH-2	6D	0.0218	2379	0.1120	0.0852	0.0011
BH-2	6E	0.0374	2381	0.1250	0.1309	0.0016
BH-2	6G	0.0302	2380	0.0798	0.1656	0.0020
BH-2	6I	0.0354	2377	0.1679	0.0924	0.0011
BH-2	6J	0.0292	2380	0.1355	0.0943	0.0011
BH-2	7A	0.0250	2379	0.1180	0.0928	0.0011
BH-2	7B	0.0187	2377	0.0958	0.0855	0.0011
BH-2	7C	0.0201	2378	0.0924	0.0953	0.0012
BH-2	7G	0.0282	2379	0.0917	0.1346	0.0016
BH-2	7H	0.0323	2378	0.1710	0.0827	0.0010
BH-2	7I	0.0429	2381	0.1682	0.1116	0.0013
BH-2	7J	0.0340	2380	0.1794	0.0830	0.0010
BH-2	8B	0.0127	2383	0.0598	0.0928	0.0013

Region	Specimen	A_{4500}	Density, gm/L	Thickness, cm	OH, wt.%	σ_{OH}, wt.%
BH-2	8C	0.0182	2383	0.0896	0.0888	0.0011
BH-2	8D	0.0322	2380	0.0832	0.1694	0.0020
BH-2	8E	0.0181	2381	0.0869	0.0911	0.0012
BH-2	8F	0.0172	2379	0.0787	0.0957	0.0012
BH-2	8G	0.0235	2382	0.0753	0.1365	0.0017
BH-2	8I	0.0551	2383	0.1333	0.1807	0.0021
BH-2	8J	0.0145	2381	0.0480	0.1322	0.0018
BH-2	9A	0.0331	2380	0.1173	0.1235	0.0015
BH-2	9B	0.0164	2378	0.0737	0.0975	0.0013
BH-2	9C	0.0274	2379	0.1278	0.0939	0.0011
BH-2	9D	0.0396	2382	0.1320	0.1312	0.0016
BH-2	9E	0.0221	2379	0.1191	0.0813	0.0010
BH-2	9F	0.0406	2379	0.1592	0.1116	0.0013
BH-2	9G	0.0318	2380	0.1630	0.0854	0.0010
BH-2	9H	0.0196	2386	0.0968	0.0884	0.0011
BH-2	9I	0.0253	2379	0.0829	0.1336	0.0016
BH-2	9J	0.0573	2380	0.1473	0.1703	0.0020
BH-2	10A	0.0268	2380	0.1059	0.1108	0.0014
BH-2	10B	0.0350	2378	0.1503	0.1020	0.0012
BH-2	10C	0.0241	2377	0.0808	0.1307	0.0016
BH-2	10D	0.0412	2377	0.1559	0.1158	0.0014
BH-2	10E	0.0341	2378	0.1667	0.0896	0.0011
BH-2	10F	0.0367	2378	0.1767	0.0910	0.0011
BH-2	10H	0.0351	2379	0.1595	0.0964	0.0011
BH-2	10J	0.0213	2389	0.0927	0.1002	0.0013
BH-2	11A	0.0378	2381	0.1858	0.0890	0.0011
BH-2	11C	0.0333	2379	0.1615	0.0903	0.0011
BH-2	11D	0.0327	2384	0.1643	0.0870	0.0010
BH-2	11E	0.0275	2378	0.1313	0.0917	0.0011
BH-2	11G	0.0323	2378	0.1206	0.1173	0.0014
BH-2	11H	0.0278	2381	0.1399	0.0869	0.0011
BH-2	11J	0.0489	2377	0.1811	0.1183	0.0014
BH-2	12B	0.0503	2381	0.2086	0.1055	0.0012
BH-2	12C	0.0727	2378	0.1998	0.1594	0.0019
BH-2	12D	0.0337	2382	0.1034	0.1425	0.0017
BH-2	12E	0.0501	2378	0.2107	0.1041	0.0012
BH-2	12F	0.0294	2379	0.1412	0.0912	0.0011
BH-2	12G	0.0347	2382	0.1758	0.0863	0.0010
BH-2	12I	0.0331	2382	0.1607	0.0901	0.0011
BH-2	12J	0.0598	2380	0.1666	0.1571	0.0018
BH-2	13A	0.0412	2380	0.1274	0.1416	0.0017
BH-2	13B	0.0457	2381	0.1313	0.1522	0.0018
BH-2	13C	0.0294	2380	0.1369	0.0940	0.0011
BH-2	13D	0.0336	2380	0.1437	0.1023	0.0012
BH-2	13F	0.0319	2381	0.1570	0.0889	0.0011
BH-2	14A	0.0300	2380	0.1457	0.0901	0.0011
BH-2	14B	0.0206	2380	0.1017	0.0886	0.0011
BH-2	14C	0.0702	2381	0.1487	0.2066	0.0024
BH-2	14D	0.0235	2389	0.0871	0.1177	0.0015
BH-2	14E	0.0295	2380	0.1489	0.0867	0.0010
BH-2	14G	0.0608	2380	0.1340	0.1986	0.0023
BH-2	15A	0.0283	2381	0.1178	0.1051	0.0013

Region	Specimen	A_{4500}	Density, gm/L	Thickness, cm	OH, wt.%	σ_{OH}, wt.%
BH-2	15D	0.0572	2378	0.1210	0.2070	0.0024
BH-2	15E	0.0248	2379	0.1274	0.0852	0.0010
BH-2	15F	0.0253	2381	0.1299	0.0852	0.0010
BH-2	15G	0.0580	2380	0.1103	0.2301	0.0027
BH-2	15I	0.0486	2380	0.1395	0.1525	0.0018
BH-2	16A	0.0177	2389	0.0601	0.1284	0.0017
BH-2	16B	0.0406	2382	0.1201	0.1479	0.0018
BH-2	16D	0.0399	2385	0.1162	0.1500	0.0018
BH-2	16E	0.0505	2379	0.1542	0.1434	0.0017
BH-2	16F	0.0249	2379	0.1235	0.0883	0.0011

Table 9. Beer-Lambert data and OH content (Bodie Hills, California; map in Stevenson et al. 2021:30-31.) (Region refers to grouping in Table 3 above.)

content and temperature to hydration rate of obsidian is obtained by taking the exponential of equation (6),

$$k = \exp[36.29 - (10005 - 354*w)/T] \qquad (7)$$

with k in μ^2/1000 years, w in wt.%, and T in Kelvins. The accuracy of the equation is $\sigma_k = 0.343$ μ^2/1000 years.

Measurement of the water content of an archaeological artifact, combined with equation (7), will provide a hydration rate specifically for that artifact, which will avoid the problem of intra-source water variation and improve OHD age accuracy (Rogers and Stevenson 2022).

References Cited

Doremus, R.H. (2002) *Diffusion of Reactive Molecules in Solids and Melts*. Wiley Interscience, New York.

Friedman, I., and W. Long (1976) Hydration Rate of Obsidian. *Science* 191(1):347-352.

Garofalini, S.H., J. Lenz, and M. Homann (2020) Molecular Mechanism of Silica Glass upon Exposure to Moisture. *Journal of the American Ceramic Society* 103: 2421-2431.

Glickman, M.E. (2000) *Diffusion in Solids: Field Theory, Solid State Principles, and Applications.* Wiley, New York.

Hughes, R.E. (1988) The Coso Volcanic Field Reexamined: Implications for Obsidian Sourcing and Dating Research. *Geoarchaeology* 3: 253-265.

Kuroda, M., S. Tachibana, N. Sakamote, S. Okumura, M. Nakamura, and N. Yuimoto (2018) Water Diffusion in Silica Glass through Pathways formed by Hydroxyls. *American Mineralogist* 103: 412-417.

Kuroda, M., S. Tachibana, N. Sakamoto, and H. Yurimoto (2019) Fast Diffusion Path for Water in Silica Glass. *American Mineralogist* 104: 385-390.

Kuroda, M., and S. Tachibana (2019) Effect of Dynamical Property of Melt on Water Diffusion in Rhyolite Melt. *ACS Earth and Space Chemistry* 3: 2058-2062.

Mazer, J.J., C.M. Stevenson, Bates, J.K., and Bradley, J.P. (1991a) The Effect of Chemical Composition on the Experimental Hydration of Obsidian Between 110 and 230°C. Argonne National Laboratory Chemical Technology Division paper ANL/CMT/PP-75148, December 1991.

Mazer, J.J., C.M. Stevenson, W.L. Ebert, and J.K. Bates (1991b) The Experimental Hydration of Obsidian as a Function of Relative Humidity and Temperature. *American Antiquity* 56(3): 504-513.

Newman, S., Stolper, E.M., Epstein, S. (1986) Measurement of Water in Rhyolitic Glasses: Calibration of an Infrared Spectroscopic Technique. *American Mineralogist* 71: 1527-1541.

Rogers, A.K. (2008) Obsidian Hydration Dating: Accuracy and Resolution Limitations Imposed by Intrinsic Water Variability. *Journal of Archaeological Science* 35: 2009-2016.

Rogers, A.K. (2011) Do Flow-Specific Hydration Rates Improve Chronological Analyses? A Case Study for Coso Obsidian. *International Association for Obsidian Studies Bulletin* 45: 14-25.

Rogers, A.K. (2015) An Equation for Estimating Hydration Rate of Obsidian from Intrinsic Water Concentration. *International Association for Obsidian Studies Bulletin* 53: 5-13.

Rogers, A.K. (2019) *Laboratory Measurement of Hydration Rate for Napa Glass Mountain Obsidian.* Maturango Museum MS83A, dated April 2, 2019. On file Maturango Museum.

Rogers, A.K., and C.M. Stevenson (2017) A New and Simple Laboratory Method for Estimating Hydration Rate of Obsidian. *Proceedings of the Society for California Archaeology* 31: 165-171.

Rogers, A.K. and C.M. Stevenson (2022) Obsidian Hydration Dating with Optical Microscopy: Is Age Accuracy Improved by Measuring Structural Water Content of a Specimen? *International Association for Obsidian Studies Bulletin* 68: 3-23.

Rogers, A.K. and R.M. Yohe II (2013) Flow-Specific Hydration Rates for Coso Obsidian. *Proceedings of the Society for California Archaeology* 27: 281-284.

Rogers, A.K. and R.M. Yohe II (2014) Obsidian Re-use at the Rose Spring Site (CA-INY-372), Eastern California: Evidence from Obsidian Hydration Studies. *Journal of California and Great Basin Anthropology* 34(2): 267-280.

Rogers, A.K., R.M. Yohe II, and K. Carroll (2018) A Re-examination of the Occupation Sequence at CA-INY-134 ("Ayers' Rock"), Eastern California. *Proceedings of the Society for California Archaeology* 32: 153-166.

Shelby, J.E. (2005) *Introduction to Glass Science and Technology*, 2nd ed. Royal Society of Chemistry, Cambridge.

Stevenson, C.M., and B.E. Scheetz (1989) Induced Hydration Rate Development of Obsidians from the Coso Volcanic Field: A Comparison of Experimental Procedures. In *Current Directions in California Obsidian Studies,* edited by R.E. Hughes, pp. 23-30. Contributions of the University of California Archaeological Research Facility No. 48., Berkeley.

Stevenson, C.M., E. Knauss, J.J. Mazer, J.K. Bates (1993) The Homogeneity of Water Content in Obsidian from the Coso Volcanic Field: Implications for Obsidian Hydration Dating. G*eoarchaeology* 8(5): 371-384.

Stevenson, C.M., M. Gottesman, and M. Macko (2000) Redefining the Working Assumptions for Obsidian Hydration Dating. *Journal of California and Great Basin Anthropology* 22(2): 223-236.

Stevenson, C.M., A.K. Rogers, and M.D. Glascock (2019) Variability in Structural Water Content and its Importance in the Hydration Dating of Cultural Artifacts. *Journal of Archaeological Science: Reports* 23: 231-242.

Stevenson, C.M., A.K. Rogers, and G. Haverstock (2021) A Brief Note on Hydration Rates for the Bodie Hills Obsidian Regional Source, Eastern California, Based on Infrared Spectroscopy and Optical Measurement. *International Association for Obsidian Studies Bulletin* 67: 30-35.

Stevenson, C.M., A.K. Rogers, and G. Haverstock (n.d.) Hydration Rates for the Bodie Hills Obsidian Regional Source, Eastern California, Based on Infrared Spectroscopy and Optical Measurement. Part II. In *Sourcing Obsidian*, edited by F.-X. LeBourdonnec, M. S. Shackley & M. Orange. Forthcoming.

Taylor, J.R. (1982) *An Introduction to Error Analysis.* University Science Books, Mill Valley, California.

Zhang, Y., E.M. Stolper, and G.J. Wasserburg (1991) Diffusion of Water in Rhyolitic Glasses. *Geochimica et Cosmochimica Acta* 55: 441-456.

Zhang, Y., R. Belcher, L. Wang, and S. Newman (1997) New Calibration of Infrared Measurement of Dissolved Water in Rhyolitic Glasses. *Geochimica et Cosmochimica Acta* 62: 3089-3100.

Zhang, Y, and H. Behrens (2000) H_2O Diffusion in Rhyolitic Melts and Glasses. *Chemical Geology* 169: 243-262.

A LIKELIHOOD-BASED METHOD FOR ASSIGNING OHD AGES TO ARCHAEOLOGICAL PERIODS

Alexander K. Rogers

Maturango Museum, Ridgecrest, California, USA

Abstract

Any chronometric method involves using a known physical process to estimate the age of an artifact or site, which amounts to evaluating a probability distribution describing the age. This is well known in the radiocarbon field, but seldom addressed in obsidian hydration dating (OHD). This is a significant oversight, since in OHD the standard deviation is large enough that the age in many cases could be assigned to more than one archaeological period with nearly equal probability, so assigning the artifact to a period based only on mean age may be misleading. Furthermore, a simple count by period may be misleading because archaeological periods are typically of unequal length, so more ages are likely to fall within a longer period than a shorter one. This paper describes a simple method for taking into account the standard deviation of the age and length of the period in a rigorous and logically consistent manner by means of likelihood analysis.

Introduction

Any chronometric method involves using a known physical process to estimate the age of an artifact or site. In each case the actual age is unknown (and formally unknowable) and the physical process is used to derive an estimate. The estimate is defined by a probability distribution, characterized by a mean – which establishes accuracy – and a standard deviation – which establishes precision. Assuming the physical process is appropriate and understood, the estimate should coincide with the actual age within some degree of confidence. In radiocarbon dating, for example, it is customary to quote the mean and two-standard-deviation interval for calibrated ages, which should contain the actual age ≈97% of the time.

In obsidian hydration dating (OHD), the mathematical models to compute standard deviation of age have been developed and published (Rogers and Yohe 2021; Rogers and Stevenson 2020) but are not in general use. The OHD age computation avoids the complications of the calibration curve relating radiocarbon years to calendar years, which typically require analysis by Monte Carlo Markov Chain methods; on the other hand, the standard deviation of age in OHD is completely dependent on post-depositional processes and is larger than for radiocarbon, typically 10 – 25 % of age (i.e. CV = 0.10 – 0.25). Thus, the standard deviation is frequently large enough that the age could be assigned to more than one archaeological period with nearly equal probability, and assigning the artifact to a period based only on mean age may be misleading. This paper takes advantage of the fact that in OHD the distribution of uncertainties about the mean is Gaussian (i.e. normal), which facilitates application of likelihood-based analysis in assigning ages to periods.

Obsidian Hydration Dating

Obsidian hydration dating ages are computed from measurement of water absorbed by the obsidian through a freshly-exposed surface. The water penetrates slowly, on the order of microns per century. The boundary between the hydrated and unhydrated volumes is visible under a
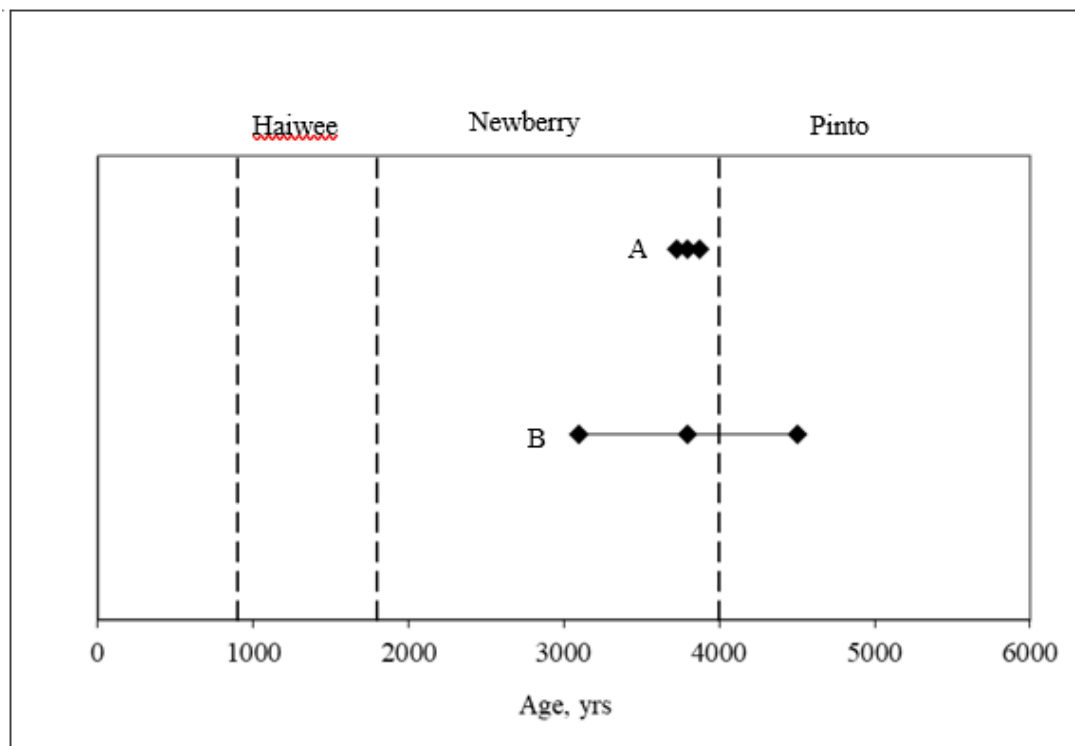
Figure 1. Two age data points are shown with mean and standard deviation, with period boundaries typical of eastern California. Case A clearly falls within the Newberry period with little ambiguity, but Case B overlaps the period boundaries.

polarized microscope, and the depth of this boundary ("hydration rim") is a measure of age. The mean, or best estimate, of age is computed by the equation

$$t = r^2/k \qquad (1)$$

where r is the hydration rim thickness (typically between 1 - 20μ) and k is the hydration rate in $μ^2$/unit time (Friedman and Smith 1960; Friedman and Long, 1976; Rogers 2007, 2012). Both r and k must be for the same geochemical source and for the same temperature. Methods have been developed to characterize the geochemical source, by XRF spectroscopy or neutron activation analysis. Hydration rates can be estimated by obsidian-radiocarbon association (Rogers and Stevenson 2020), use of temporally-sensitive artifacts as time markers (Rogers and Duke 2014a), laboratory hydration (Rogers and

Duke 2011, 2014b; Stevenson et al. 1998) or by measurement of intrinsic water content (Rogers 2015; Rogers and Stevenson 2017; Stevenson et al. 2018). It is known that variations in obsidian intrinsic water content have a major effect on hydration rate (Ambrose and Stevenson 2004; Rogers and Yohe 2021; Stevenson et al. 2000, 2018), but only the last-mentioned method above takes it into account. Methods to compute temperature corrections have also been developed and published (Rogers 2007, 2012).

Any measurement has experimental uncertainties which lead to errors in the result. In the case of OHD, six significant sources of error have been identified: measurement of the hydration rim; errors in the hydration rate ascribed to a geochemical source; uncertainties in estimating temperature history; intra-source variations in intrinsic water content; uncertainties due to
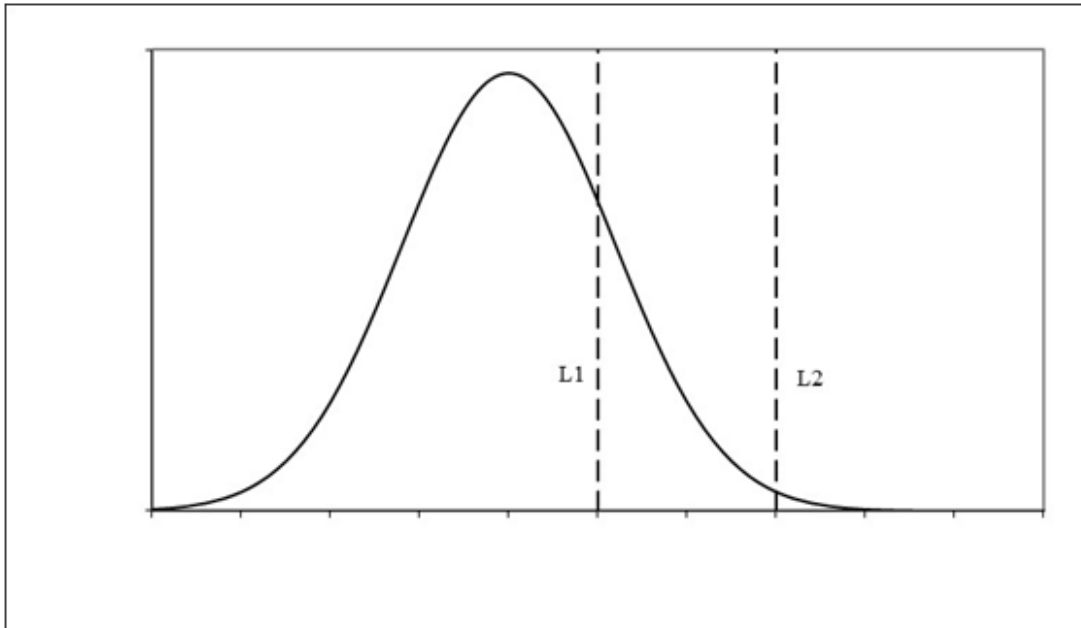
Figure 2. A typical age data point overlapping boundaries. The area under the curve between L1 and L2 is the probability that the actual age falls within these limits.

fluctuations in relative humidity; and uncertainties caused by site formation effects (Rogers 2008, 2010; Rogers and Stevenson 2020). A method to quantify these uncertainties has been developed and published (Rogers and Yohe 2021), so that a numerical value of standard deviation can be estimated. Since OHD, like optically-stimulated luminescence and unlike radiocarbon, depends on post-depositional processes, the standard deviation of age is a function of age itself. On the other hand, the coefficient of variation of the age is constant, typically on the order of 10-25% of the mean age. The distribution of the age errors in OHD is Gaussian (i.e. normally distributed), unlike radiocarbon, in which the calibration curve distorts the Gaussian distribution of the radiocarbon age.

Assigning Ages to Archaeological Periods

In most archaeological analyses, ages are assigned to periods simply by "binning", placing the mean values of the ages into "age bins" representing periods. If the standard

deviation of the age is small, this can be a reasonable method (case A in Figure 1); however, if the standard deviation is large it can lead to ambiguities (case B in Figure 1), in which the age could be assigned to either period with nearly equal probability.

The solution to the ambiguity is to describe the age by the normal distribution function (Figure 2) and compute its contribution to each period. For an age described by a mean (m) and standard deviation (s), the normal probability density function is

$$p(t) = \{1/[s*\sqrt{(2*\pi)}]\}\exp[-(t-m)^2/(2*s^2)] \quad (2)$$

where p(t) is the probability that the age t lies between t and t + dt. Thus, the probability that the age falls between L_1 and L_2 is

$$p(L_1,L_2) = \{1/[s*\sqrt{(s*\pi)}]\}\int\exp[-(t-m)^2/(2*s^2)]dt \quad (3)$$

where the integral is taken between t = L_1 and t = L_2. In Figure 2, P(L_1, L_2) is the area under the curve between L_1 and L_2. The integral of

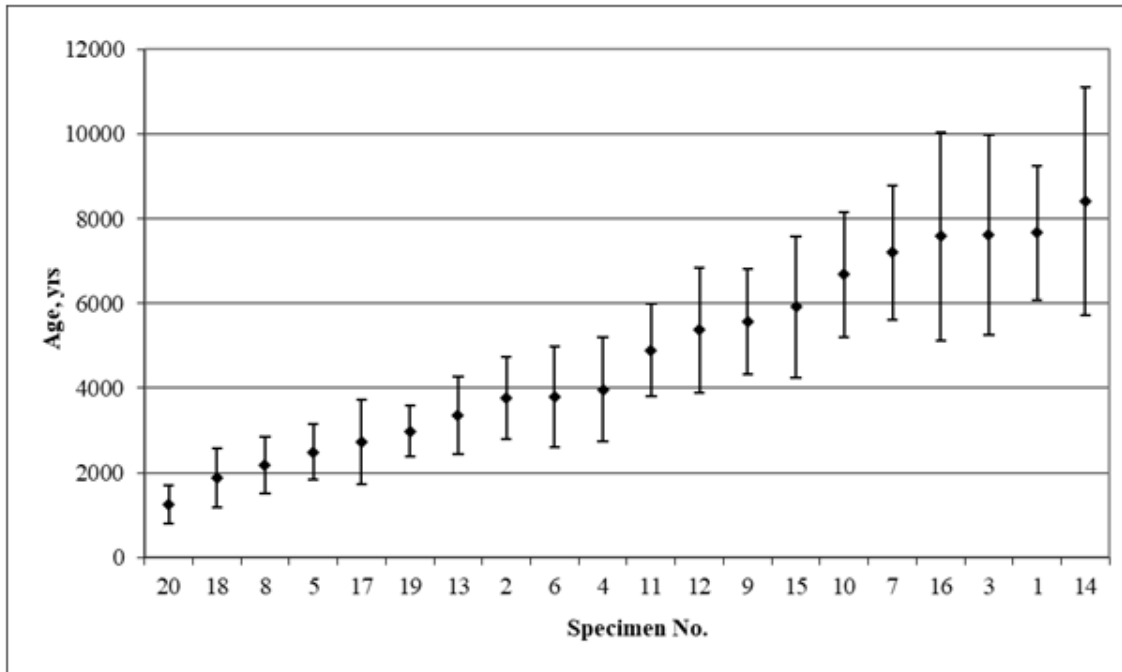**Figure 3.** Age data from Table 1, plotted in ascending order.

the normal distribution is the error function (erf), defined as

$$erf(L)=\{1/[s*\sqrt{(s*\pi)}]\}\int exp[-(t-m)^2/(2*s^2)]dt \quad (4)$$

with the integral taken from $-\infty$ to L. Thus, the probability that the age falls within the interval L_1 to L_2 is simply

$$p(L_1, L_2)=erf(L_2)-erf(L_1) \quad (5)$$

where

$$L_n = (L_n - m)/[(sqrt(2)*s] \quad (6)$$

and n can equal 1 or 2. The error function can be looked up in published tables (e.g. Lindgren 1962: 392, Table I), or accessed by a function call in MS Excel or applications such as MatLab or Mathematica.

For a single artifact, the probability distribution across the periods is obtained by computing the probability for each period by equations (5) and (6); in this case

"probability" is the appropriate term, since the sum of the probabilities across the periods is unity (i.e. normalized to one). If there is more than one artifact, the distribution of ages by period is obtained by computing the probability for each artifact for each period by equations (5) and (6), and then summing the results by period. The resulting distribution is a "likelihood" rather than "probability", because the sum of the probabilities across the periods equals the number of specimens and thus is not normalized to one. The interpretation of the likelihood value for any given period is the most likely number of ages that fall within the period, which does not have to be an integral value.

Significance of Age Count in a Period

Assigning ages to an archaeological period by the method above gives the likelihood value for the period; however, archaeological periods are typically of unequal length, so even if the distribution of ages were uniform, more ages will fall within a longer period than a shorter one. Thus, the

Seq. No.	Age, yrs	Std. dev. age, yrs
1	7667	1587
2	3773	972
3	7625	2372
4	3962	1233
5	2491	667
6	3794	1190
7	7206	1584
8	2175	669
9	5576	1240
10	6683	1483
11	4892	1098
12	5365	1472
13	3352	927
14	8416	2704
15	5913	1659
16	7592	2463
17	2722	1001
18	1875	698
19	2980	608
20	1252	459

Table 1. Age data for example.

likelihood per period, while interesting, does not give an indication of intensity of use or occupation during that period. This shortcoming can be resolved by dividing the likelihood by the length of the archaeological period; if the length of the periods is in millennia, the result is a likelihood per millennium, which is a measure of intensity of occupation or use during that period.

Period	Start, years BP	Length, millennia
Proto-Historic	150	0.75
Marana	900	0.9
Haiwee	1800	2.2
Newberry	4000	4.0
Pinto	8000	2.0
Lake Mojave	10000	2.0
Paleoindian	12000	11.0
Pleistocene-Holocene Transition	23000	-

Table 2. Archaeological period boundaries for example.

Example

An example clarifies the process, using the data set in Table 1. The ages are plotted in Figure 3, with their standard deviations, showing the overlap which suggests a histogram based on mean ages alone is inadequate. The period definitions typical of Owens Valley in eastern California are used (Table 2), although others could be substituted. Thus, the computation in equation (5) is performed using the age data in Table 1 and the period boundaries in Table 2. Table 3 shows the results of a simple binning by means alone, plus likelihood/period and likelihood/ millennium, both including standard deviations.

Figure 4 graphically compares the likelihood/period based on only the mean, with likelihood/period based on mean plus standard deviation. Note that although there were no specimens with mean ages falling into the Marana or Proto-historic periods, including standard deviation shows that there is still a non-zero likelihood that actual ages fell within these periods. Including standard deviations fills in the periods.

Figure 5 illustrates the effects of normalizing the likelihood by the length of each period, taking standard deviation into account in both cases. The data for likelihood/period show a major spike in the Pinto and Newberry periods with much lower likelihood in the Haiwee period. However, the likelihood/ millennia data show that much of the Pinto-Newberry spike is caused by the length of the periods rather than greater likelihood; in fact the likelihood/millennia for the Haiwee period is actually greater than for the Pinto period. Thus, an archaeologist interpreting this data set would infer that the Pinto period contains the highest likelihood of OHD dates, but the actual peak in intensity of use was in the Newberry period and that use probably continued into the succeeding periods.
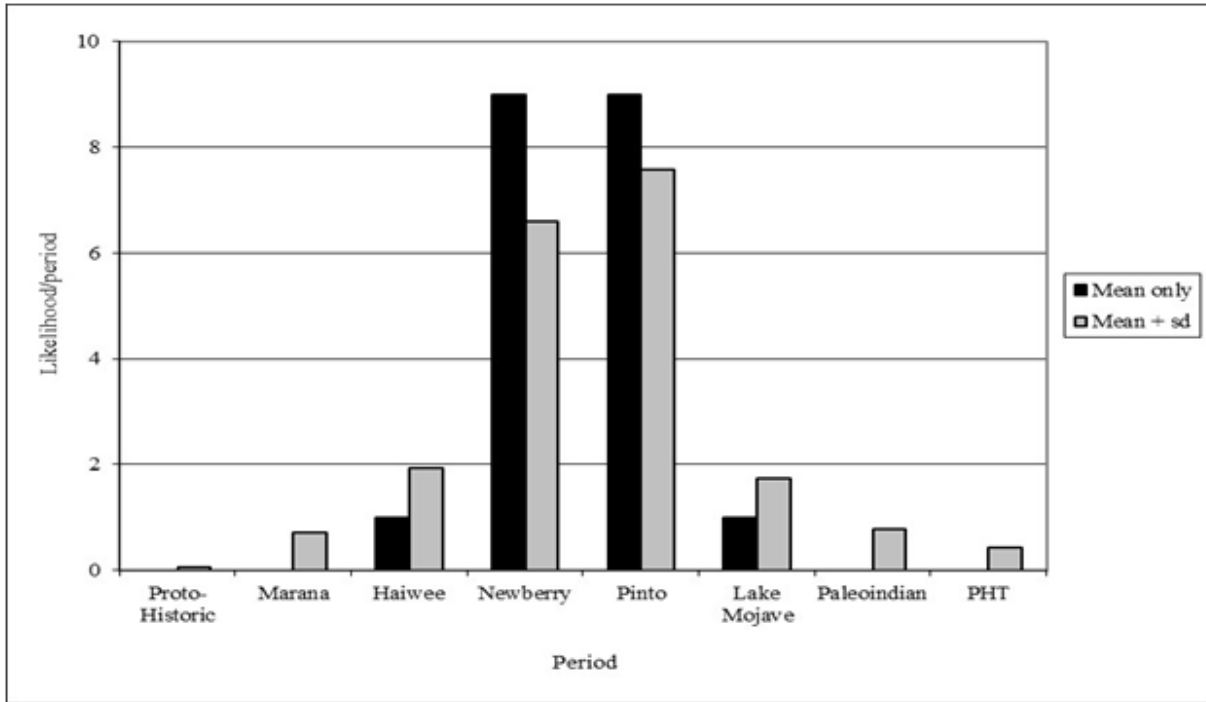
Figure 4. Histogram of likelihood/period, comparing the computation with mean only and mean plus standard deviation.
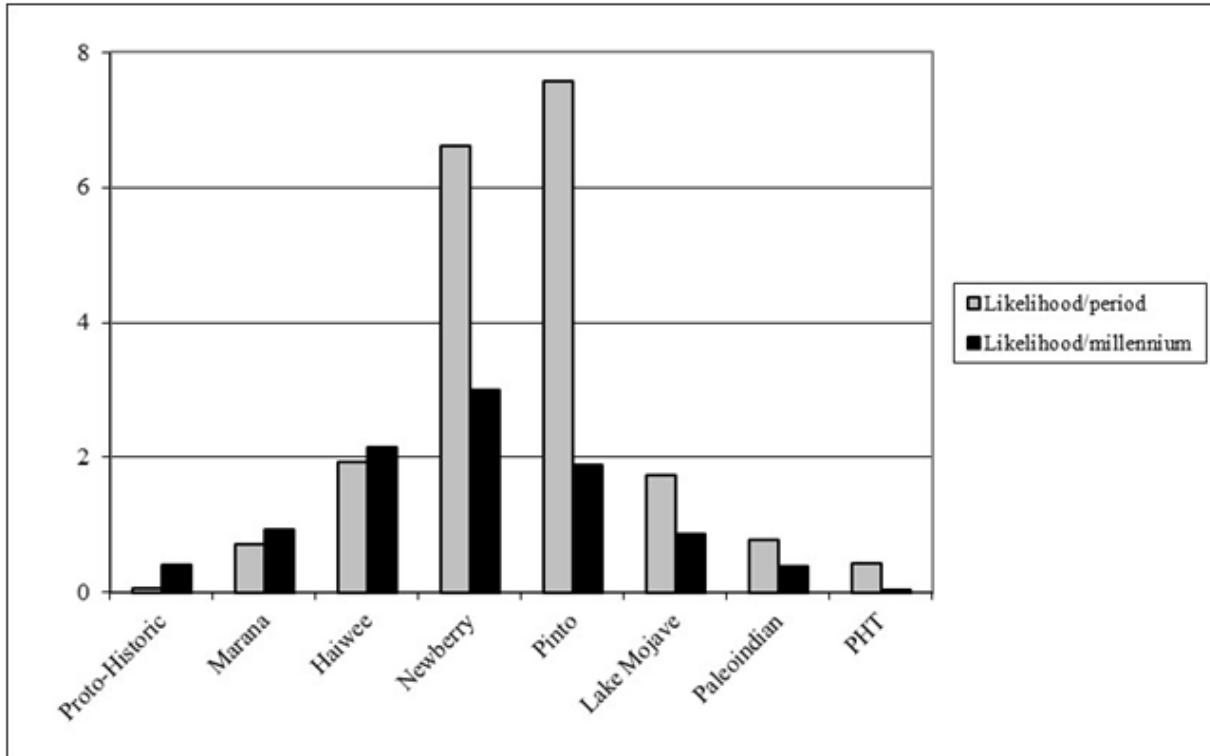

Figure 5. Histogram of likelihood/period compared with likelihood/millennium.

Period	Likelihood/ period based on mean only	Likelihood/ period, based on mean + sd	Likelihood/ millennium, based on mean + sd
Proto-Historic	0	0.06	0.41
Marana	0	0.70	0.94
Haiwee	1	1.94	2.15
Newberry	9	6.60	3.00
Pinto	1	7.58	1.89
Lake Mojave	0	1.74	0.97
Paleoindian	0	0.77	0.38
P-H Transition	0	0.43	0.04

Table 3. Example output.

Computer Code

Although the computation in equation (5) can be performed with MS Excel, the process is tedious, so a program in MatLab has been developed. The code reads an input file in comma-separated variable (.csv) format, which contains, for each data point, a sequence number, a mean age, and a standard deviation in the format of Table 1. It computes probabilities for each specimen based on the period boundaries of Table 2, although these can be changed in the code to reflect other definitions. It outputs a .csv file with the aggregate likelihood for each period, plus a check-sum to verify all data were read correctly. It also computes the aggregate likelihood/millennium. The MatLab code is at the end of this article, which also shows the printed output for this example.

Concluding Observations

Ages determined by OHD tend to have fairly large standard deviations. The analytical method proposed here provides a more rigorous tool for understanding OHD dates in their archaeological context than simply examining the mean ages. It takes advantage of the Gaussian (normal) nature of the distribution of experimental error, which simplifies the computation, and can be performed by either MS Excel or an application such as MatLab or Mathematica. Properly used, it can provide insights into the intensity of use of a site in any given archaeological period.

References Cited

Ambrose, W.R., and C.M. Stevenson (2004) Obsidian Density, Connate Water, and Hydration Dating. *Mediterranean Archaeology and Archaeometry* 4(2): 5-16.

Friedman, I., and R. Smith (1960) A New Method of Dating Using Obsidian; Part 1, the Development of the Method. *American Antiquity* 25(4): 476-522.

Friedman, I., and W. Long (1976) Hydration Rate of Obsidian. *Science* 191(1):347-352.

Lindgren, B.W. (1962) *Statistical Theory*. MacMillan, New York

Rogers, A.K. (2007) Effective Hydration Temperature of Obsidian: A Diffusion-Theory Analysis of Time-Dependent Hydration Rates. *Journal of Archaeological Science* 34: 656-665.

Rogers, A.K. (2008) Obsidian Hydration Dating: Accuracy and Resolution Limitations Imposed by Intrinsic Water Variability. *Journal of Archaeological Science* 35: 2009-2016.

Rogers, A.K. (2010) Accuracy of Obsidian Hydration Dating Based on Radiocarbon Association and Optical Microscopy. *Journal of Archaeological Science* 37: 3239-3246.

Rogers, A.K. (2012) Temperature Correction for Obsidian Hydration Dating, In *Obsidian and Ancient Manufactured Glasses*, edited by I. Liritzis and C.M. Stevenson, pp. 46-55. University of New Mexico Press, Albuquerque.

Rogers, A.K. (2015) An Equation for Estimating Hydration Rate of Obsidian from Intrinsic Water Concentration. *International Association for Obsidian Studies Bulletin* 53: 5-13.

Rogers, A.K., and D. Duke (2011) An Archaeologically Validated Protocol for Computing Obsidian Hydration Rates from Laboratory Data. *Journal of Archaeological Science* 38: 1340-1345.

Rogers, A.K., and D. Duke (2014a) Estimating Obsidian Hydration Rates from Temporally-Sensitive Artifacts: Method and Archaeological Examples. *International Association for Obsidian Studies Bulletin* 51: 31-38.

Rogers, A.K., and D. Duke (2014b) Unreliability of the Induced Hydration Method with Abbreviated Hot-Soak Protocols. *Journal of Archaeological Science* 52: 428 – 435.

Rogers, A.K., and C.M. Stevenson (2017) A New and Simple Laboratory Method for Estimating Hydration Rate of Obsidian. *Proceedings of the Society for California Archaeology* 31: 165-171.

Rogers, A.K., and C.M. Stevenson (2020) Archaeological Age Computation Based on Obsidian Hydration: A Summary of the Current State of the Art. *International Association for Obsidian Studies Bulletin* 63: 2-44.

Rogers, A.K. and R.M. Yohe II (2021) An Equation to Compute Accuracy of Obsidian Hydration Dating Ages. *International Association for Obsidian Studies Bulletin* 67: 5-14.

Stevenson, C.M., J.J. Mazer, and B.E. Scheetz (1998) Laboratory Obsidian Hydration Rates: Theory, Method, and Application. In *Archaeological Obsidian Studies: Method and Theory. Advances in Archaeological and Museum Science*, Vol. 3, edited by M.S. Shackley, pp.181-204. Plenum Press. New York.

Stevenson, C.M., M. Gottesman, and M. Macko (2000) Redefining the Working Assumptions for Obsidian Hydration Dating. *Journal of California and Great Basin Anthropology* 22(2): 223-236.

Stevenson, C.M., A.K. Rogers, and M.D. Glascock (2019) Variability in Structural Water Content and its Importance in the Hydration Dating of Cultural Artifacts. *Journal of Archaeological Science: Reports* 23: 231-242.

```
% Program TemporalBinsMod
% Assigns OHD dates to temporal bins based on mean and std. dev.
clear
Hi = 'Hist';
Ma = 'Marana';
Ha = 'Haiwee';
Ne = 'Newberry';
Pn = 'Pinto';
LM = 'LakeMojave';
PI = 'Palepoindian';
PH = 'PHT';
PR = 'Prior';
TI = [Hi,Ma,Ha,Ne,Pn,LM,PI,PH,PR];
for k = 1:9
    ABS(k) = 0;
end
% Temporal bins
    L(1) = 0;      %Present
    L(2) = 150;    %Historic period start
    L(3) = 900;    %Marana period start
    L(4) = 1800;   %Haiwee period start
    L(5) = 4000;   %Newberry period start
    L(6) = 8000;   %Pinto period start
    L(7) = 10000;  %Lake Mojave period start
    L(8) = 12000;  %Paleoindian period start
    L(9) = 23000;  %LGM, PHT start
    L(10)= 50000;
for i = 1:9
    DL(i)= (L(i+1)-L(i))/1000;
end
%
%************************************************************************
% Read input data
INDATA = csvread('C:\MATLAB701\work\TempBinsIn.csv');
LL = size(INDATA,1);
for jj = 1:LL % jj is index for sequence number.
   SN  = INDATA(jj,1); %Sequence Number
   age = INDATA(jj,2); %Mean age, cal BP
   sda = INDATA(jj,3); %Std. Dev of age, yrs
%
%************************************************************************

    for k = 1:9
        t(k) =   (age-L(k))/(2*sda);
        A = abs(erf(t(k)));
        t(k+1) = (age-L(k+1))/(2*sda);
        B = abs(erf(t(k+1)));
        if ((age >= L(k)) & (age <= L(k+1)));
            AB(k)= (A + B)/2;
        else
            AB(k) = abs(A - B)/2;
        end
        ABS(k) = ABS(k)+AB(k);
    end
end
```

```
for k = 1:9
    NP(k)        = ABS(k);
    NT(k)        = ABS(k)/DL(k);
    OUTDATA(k,1) = k;
    OUTDATA(k,2) = NP(k);
    OUTDATA(k,3) = NT(k);
end
dlmwrite('TempBinsOut.csv', OUTDATA, ',')
fprintf('Run Complete\n')
fprintf('\n')
fprintf('Date distribution by period\n')
fprintf('Historic period.......................%6.2f\n' ,NP(1))
fprintf('Marana Period.........................%6.2f\n', NP(2))
fprintf('Haiwee Period.........................%6.2f\n', NP(3))
fprintf('Newberry Period.......................%6.2f\n', NP(4))
fprintf('Pinto Period..........................%6.2f\n', NP(5))
fprintf('Lake Mojave Period....................%6.2f\n', NP(6))
fprintf('Paleoindian Period....................%6.2f\n', NP(7))
fprintf('Pleistocene-Holocene Transition.......%6.2f\n', NP(8))
fprintf('Prior.................................%6.2f\n', NP(9))
fprintf('\n')
fprintf('Date distribution per millennium\n')
fprintf('Historic period.......................%6.2f\n' ,NT(1))
fprintf('Marana Period.........................%6.2f\n', NT(2))
fprintf('Haiwee Period.........................%6.2f\n', NT(3))
fprintf('Newberry Period.......................%6.2f\n', NT(4))
fprintf('Pinto Period..........................%6.2f\n', NT(5))
fprintf('Lake Mojave Period....................%6.2f\n', NT(6))
fprintf('Paleoindian Period....................%6.2f\n', NT(7))
fprintf('Pleistocene-Holocene Transition.......%6.2f\n', NT(8))
fprintf('Prior.................................%6.2f\n', NT(9))
fprintf('\n')
```

                        EXAMPLE OUTPUT TEXT
              (note: data are also written to a .csv file)

```
Date distribution by period
Historic period.......................  0.06
Marana Period.........................  0.70
Haiwee Period.........................  1.94
Newberry Period.......................  6.60
Pinto Period..........................  7.58
Lake Mojave Period....................  1.74
Paleoindian Period....................  0.77
Pleistocene-Holocene Transition.......  0.43
Prior.................................  0.00

Date distribution per millennium
Historic period.......................  0.41
Marana Period.........................  0.94
Haiwee Period.........................  2.15
Newberry Period.......................  3.00
Pinto Period..........................  1.89
Lake Mojave Period....................  0.87
Paleoindian Period....................  0.38
Pleistocene-Holocene Transition.......  0.04
Prior.................................  0.00
```

ABOUT OUR WEB SITE

The IAOS maintains a website at http://www.deschutesmeridian.com/IAOS/ The site has some great resources available to the public, and our webmaster, Craig Skinner, continues to update the list of publications and must-have volumes.

You can now become a member online or renew your current IAOS membership using PayPal. Please take advantage of this opportunity to continue your support of the IAOS.

Other items on our website include:

- World obsidian source catalog
- Back issues of the *Bulletin.*
- An obsidian bibliography
- An obsidian laboratory directory
- Photos and maps of some source locations
- Links

Thanks to Craig Skinner for maintaining the website. Please check it out!

CALL FOR ARTICLES

Submissions of articles, short reports, abstracts, or announcements for inclusion in the *Bulletin* are always welcome. We accept submissions in MS Word. Tables should be submitted as Excel files and images as .jpg files. Please use the *American Antiquity* style guide for formatting references and bibliographies. http://www.saa.org/Portals/0/SAA%20Style%20Guide_Updated%20July%202018.pdf

Submissions can also be emailed to the *Bulletin* at IAOS.Editor@gmail.com Please include the phrase "IAOS Bulletin" in the subject line. An acknowledgement email will be sent in reply, so if you do not hear from us, please email again and inquire.

Deadline for Issue #70 is May 1, 2023.

Email or mail submissions to:

Dr. Carolyn Dillian
IAOS Bulletin, Editor
Spadoni College of Education & Social Science
Coastal Carolina University
P.O. Box 261954
Conway, SC 29528
U.S.A.
IAOS.Editor@gmail.com

Inquiries, suggestions, and comments about the *Bulletin* can be sent to IAOS.Editor@gmail.com Please send updated address/email information to Lucas Martindale Johnson at lucas@farwestern.com

MEMBERSHIP

The IAOS needs membership to ensure success of the organization. To be included as a member and receive all of the benefits thereof, you may apply for membership in one of the following categories:

Regular Member: $20/year*
Student Member: $10/year or FREE with submission of a paper to the *Bulletin* for publication. Please provide copy of current student identification.
Lifetime Member: $200

Regular Members are individuals or institutions who are interested in obsidian studies, and who wish to support the goals of the IAOS. Regular members will receive any general mailings; announcements of meetings, conferences, and symposia; the *Bulletin*; and papers distributed by the IAOS during the year. Regular members are entitled to vote for officers.

*Membership fees may be reduced and/or waived in cases of financial hardship or difficulty in paying in foreign currency. Please contact the Secretary-Treasurer with a short explanation regarding lack of payment.

NOTE: The IAOS asks that all payments be made using the PayPal link on our website: http://www.deschutesmeridian.com/IAOS/membership.html

For more information about membership in the IAOS, contact our Secretary-Treasurer:

Lucas Martindale Johnson
lucas@farwestern.com

Membership inquiries, address changes, or payment questions can also be emailed to lucas@farwestern.com

---

ABOUT THE IAOS

The International Association for Obsidian Studies (IAOS) was formed in 1989 to provide a forum for obsidian researchers throughout the world. Major interest areas include: obsidian hydration dating, obsidian and materials characterization ("sourcing"), geoarchaeological obsidian studies, obsidian and lithic technology, and the prehistoric procurement and utilization of obsidian. In addition to disseminating information about advances in obsidian research to archaeologists and other interested parties, the IAOS was also established to:

1. Develop standards for analytic procedures and ensure inter-laboratory comparability.
2. Develop standards for recording and reporting obsidian hydration and characterization results
3. Provide technical support in the form of training and workshops for those wanting to develop their expertise in the field.
4. Provide a central source of information regarding the advances in obsidian studies and the analytic capabilities of various laboratories and institutions